Proceedings of ASME 2019
Dynamic Systems and Control Conference
DSCC2019
October 09-11, 2019, Park City, UT, USA

DSCC2019-9117

GLOBAL-POSITION TRACKING CONTROL OF MULTI-DOMAIN PLANAR BIPEDAL ROBOTIC WALKING

Yuan Gao
Ph.D. student
Department of Mechanical Engineering
University of Massachusetts Lowell
Lowell, MA 01854
Email: yuan_gao@student.uml.edu

Yan Gu *
Ph.D., Assistant Professor
Department of Mechanical Engineering
University of Massachusetts Lowell
Lowell, MA 01854
Email: yan_gu@uml.edu

ABSTRACT

Reliable global-position tracking control is crucial for bipedal robots to perform high-level tasks such as multi-agent coordination and dynamic-obstacle avoidance. Here, a robot's global position refers to its position in the environment. In this study, a control approach that can provably achieve satisfactory global-position tracking is proposed for bipedal robots with a general multi-domain gait, which consists of walking phases (domains) of full actuation, over actuation, and underactuation. The derivation of the proposed control law begins with full-order modeling of the hybrid, nonlinear walking dynamics. Based on the full-order model, input-output linearizing control is synthesized, which can achieve exponential global-position tracking within the fully-actuated and the over-actuated domains but may result in uncontrolled internal dynamics within the underactuation domain. To enable reliable global-position tracking for the overall hybrid closed-loop system, the construction of multiple Lyapunov functions is employed to derive sufficient conditions under which the tracking performance of the proposed control law can be provably guaranteed. Finally, simulations of a planar bipedal robot were performed to demonstrate the effectiveness of the proposed control approach.

*Address all correspondence to this author.

INTRODUCTION

Human walking is naturally multi-domain consisting of fully-actuated, underactuated, and over-actuated domains [1]. A bipedal locomotor is fully-actuated when the support foot has a full, static contact with the ground, is underactuated when only the support-foot toe contacts the ground, and is over-actuated when the swing-foot heel touches the ground while the support-foot toe is still in contact. Previous studies have revealed that humans utilize the underactuated domain of their multi-domain gait to enhance walking agility [2]. During the underactuated domain, the support-foot toe works as a pivot to rotate the whole body to fall down, accelerating the body to achieve higher walking speed and allowing the legs to reach a longer step. During the fully- and over-actuated domains, the locomotor regains a secured contact with the ground and is thus able to resume reliable tracking of various desired motions for achieving high versatility. Although the rolling motion of the support foot is key to the inherent versatility and agility of multi-domain walking and is deceptively easy for humans to realize, the resulting underactuated walking phases can present a difficult challenge for bipedal robotic walking control.

To address the control challenge of achieving versatile and agile bipedal robotic walking, various control frameworks have been proposed. Among them, the Zero-Moment-Point (ZMP) approach [3] is the most widely applied one, which has been utilized to achieve high walking versatility based on reduced-order modeling and the ZMP balance criterion [4, 5].

© 2019 by ASME

Another intensively studied control approach, which is called the Hybrid-Zero-Dynamics (HZD) approach [6, 7], has been developed to achieve provable stabilization and high agility of walking, including fully-actuated [8], underactuated [9, 10], and multi-domain [11, 12, 13] walking. Recently, researchers have investigated speed regulation [14] and gait library [15] based on the HZD approach to improve walking versatility. These control strategies have been successfully implemented on a variety of bipedal robots, such as DURUS [12], AMBER2 [13], Cassie [16], and NAO [8]. The HZD framework has also been extended to the motion control of exoskeletons [17].

To simultaneously achieve versatile and agile bipedal robotic walking, we have theoretically derived a control approach that achieves exponential global-position tracking for fully actuated planar bipedal robots [18, 19]. Later on, this control approach has been extended from a planar to a three-dimensional (3-D) fully-actuated robot [20], which has been validated through both 3-D realistic simulations and experiments on an NAO bipedal humanoid robot [21].

Inspired by the high performance of multi-domain human walking, this study will theoretically extend our previous global-position tracking control approach from (single-domain) fully-actuated walking to multi-domain walking for enhancing the walking versatility and agility of bipedal robots. A complete cycle of a multi-domain gait consists of a fully-actuated domain, an underactuated domain, and an over-actuated domain. Within the fully-actuated and the over-actuated domains, an input-output linearizing control law will be utilized to exponentially drive the tracking error of the desired trajectories, which include the desired global-position trajectory, to zero. Within the underactuated domain, the robot's degrees of freedom cannot all be directly controlled to track the desired trajectories due to the lack of control authority, and thus internal dynamics may exist under input-output linearizing control. Since it may not be realistic to realize exponential trajectory tracking within the underactuated domain, the controller design for the underactuated domain aims to achieve a bounded tracking error rather than exponential tracking. Besides underactuation, another controller design challenge is presented by the discrete behaviors of a foot-landing impact, which cannot be directly controlled due to its infinitesimally short duration. Thus, the tracking performance of the closed-loop control system will be formally analyzed based on Lyapunov theory [22] so as to derive sufficient conditions under which the proposed control law can provably guarantee the tracking performance of the overall hybrid multi-domain walking system.

This paper is structured as follows. Section 1 presents the hybrid, full-order model of multi-domain walking dynamics. The proposed trajectory tracking control law is explained in Section 2. In Section 3, Lyapunov-based stability analysis is presented. Section 4 shows MATLAB [23] simulation results to demonstrate the effectiveness of our proposed control strategy.

1 FULL-ORDER DYNAMIC MODELING OF MULTI-DOMAIN WALKING

In this section, a full-order model of multi-domain bipedal robotic walking is presented, which provides a faithful description of the dynamic behaviors for all degrees of freedom (DOFs) of the robot. Thanks to the high accuracy of a full-order model in representing the true dynamics of bipedal robotic walking, a controller design that is valid for a full-order model will also be effective for the real robot. Therefore, this model will serve as a basis for the proposed controller design in Section 2.

The generalized coordinates of a floating-based planar bipedal robot with n revolute joints can be denoted as

$$\mathbf{q} = \left[\mathbf{q}_b^T, q_1, ..., q_n\right]^T \in Q, \tag{1}$$

where $Q \subset \mathbb{R}^{n+3}$ is the configuration space, $\mathbf{q}_b := [x_b, z_b, \theta_b]^T \in \mathbb{R}^3$ is the floating-base position and orientation with respect to the world coordinate frame, which is used to represent the robot's global position and orientation in this study, and $q_1, ..., q_n$ are the robot's joint angles.

1.1 Walking Domain Description

The multi-domain walking considered in this study consists of three domains, which are fully-actuated, underactuated, and over-actuated domains. Figure 1 shows the three domains and the transitions between them. For simplicity and without loss of generality, it is assumed that the only contact points on each foot are the toe and the heel [11]. Let n_b, n_h, and n_a denote the number of DOFs of a robot's floating base, the number of holonomic constraints within a domain, and the number of independent actuators, respectively. Note that $n_b = 3$ for planar robots and that $n_a = n$ when the robot has n independent actuators. The number of DOFs of the robot can be computed as DOF$= (n+n_b) - n_h$. The complete description of each domain is given below:

Fully-Actuated (FA) Domain: In this domain, there are three holonomic constraints, i.e., $n_h = 3$, because the support foot keeps a static, full contact with the ground. Thus, DOF$= (n + n_b) - n_h = n = n_a$; i.e., the number of DOFs equals that of actuators, which indicates that the robot is fully-actuated.

Underactuated (UA) Domain: In this domain, there are two holonomic constraints, i.e., $n_h = 2$, because only the support-foot toe touches the ground. Thus, DOF$= (n+n_b) - n_h = n+1 > n_a$, i.e., the number of DOFs is greater than that of actuators, which indicates that the robot is underactuated.

Over-Actuated (OA) Domain: In this domain, there are four holonomic constraints, i.e., $n_h = 4$, because both the leading-foot toe and the trailing-foot heel touch the ground. Thus, DOF$=$ $(n+n_b) - n_h = n-1 < n_a$; i.e., the number of DOFs is less than that of actuators, which indicates that the robot is over-actuated.

© 2019 by ASME

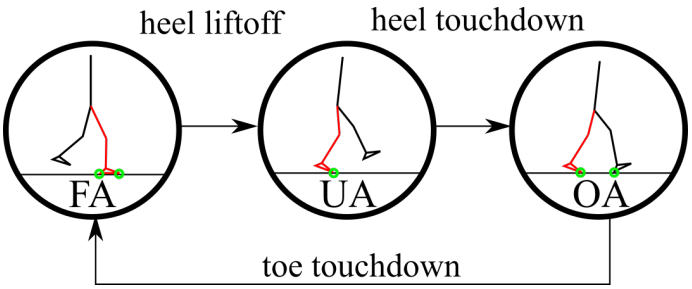

FIGURE 1. Illustration of the three domains and the transitions between them within a multi-domain walking step. The red lines and the green circles indicate the support foot and its contract points with the ground, respectively.

1.2 Hybrid Multi-Domain Walking Dynamics

The full-order model of multi-domain walking dynamics is naturally hybrid because walking inherently involves both continuous motion (e.g. foot swinging) and discrete behaviors (e.g., landing impacts).

Continuous Dynamics: With Lagrange's method, the continuous dynamics of multi-domain walking can be obtained as

$$\mathbf{M}(\mathbf{q})\ddot{\mathbf{q}} + \mathbf{c}(\mathbf{q},\dot{\mathbf{q}}) = \mathbf{B}\mathbf{u} + \mathbf{J}^T\mathbf{F}_{ext}, \tag{2}$$

where $\mathbf{J}(\mathbf{q}) : Q \to \mathbb{R}^{2\times(n+3)}$ is the Jacobian matrix, $\mathbf{M}(\mathbf{q}) : Q \to \mathbb{R}^{(n+3)\times(n+3)}$ is the inertia matrix, $\mathbf{c}(\mathbf{q},\dot{\mathbf{q}}) : TQ \to \mathbb{R}^{(n+3)}$ is the sum of Coriolis, centrifugal, and gravitational terms, $\mathbf{B} \in \mathbb{R}^{(n+3)\times n_a}$ is the input matrix, and $\mathbf{u} \in U \subset \mathbb{R}^{n_a}$ is the joint-torque vector (U is the set of admissible control input). Here, $\mathbf{F}_{ext}$ is the vector of external forces applied at the contact points. The dimension of $\mathbf{F}_{ext}$ depends on the walking domain: a) $\mathbf{F}_{ext} \in \mathbb{R}^3$ within the fully-actuated domain; b) $\mathbf{F}_{ext} \in \mathbb{R}^2$ within the underactuated domain; and c) $\mathbf{F}_{ext} \in \mathbb{R}^4$ within the over-actuated domain. The holonomic constraints can be expressed as

$$\mathbf{J}\ddot{\mathbf{q}} + \dot{\mathbf{J}}\dot{\mathbf{q}} = \mathbf{0}. \tag{3}$$

From Eqs. (2) and (3), the continuous dynamics can be compactly expressed as

$$\mathbf{M}(\mathbf{q})\ddot{\mathbf{q}} + \bar{\mathbf{c}}(\mathbf{q},\dot{\mathbf{q}}) = \bar{\mathbf{B}}(\mathbf{q})\mathbf{u}, \tag{4}$$

where the derivation of $\bar{\mathbf{c}}$ and $\bar{\mathbf{B}}$ is similar to our previous work [21] and is thus omitted due to the space limitation.

Switching surfaces: A switching event connects two successive domains [13]. Three switching surfaces are required to connect three domains into a multi-domain walking cycle (see Fig. 1).

The switching surfaces $S_{F\to U}$, $S_{U\to O}$, and $S_{O\to F}$ connect the FA to the subsequent UA, the UA to the subsequent OA, and the OA to the subsequent FA, respectively, which can be expressed as:

$$\begin{aligned} S_{F\to U}(\mathbf{q},\dot{\mathbf{q}},\mathbf{u}) &:= \{(\mathbf{q},\dot{\mathbf{q}},\mathbf{u}) \in TQ\times U : F_{ext,z}(\mathbf{q},\dot{\mathbf{q}},\mathbf{u}) = 0, \\ &\qquad \dot{F}_{ext,z}(\mathbf{q},\dot{\mathbf{q}},\mathbf{u}) < 0\}; \\ S_{U\to O}(\mathbf{q},\dot{\mathbf{q}}) &:= \{(\mathbf{q},\dot{\mathbf{q}}) \in TQ : z_{swh}(\mathbf{q}) = 0, \dot{z}_{swh}(\mathbf{q},\dot{\mathbf{q}}) < 0\}; \\ S_{O\to F}(\mathbf{q},\dot{\mathbf{q}}) &:= \{(\mathbf{q},\dot{\mathbf{q}}) \in TQ : z_{swt}(\mathbf{q}) = 0, \dot{z}_{swt}(\mathbf{q},\dot{\mathbf{q}}) < 0\}, \end{aligned}$$

where $F_{ext,z} : TQ\times U \to \mathbb{R}$ is the vertical component of the external force applied on the support-foot heel, $z_{swh} : Q \to \mathbb{R}$ is the height of swing-foot heel above the walking surface, and $z_{swt} : Q \to \mathbb{R}$ is the height of leading-foot toe above the walking surface.

Reset Maps: A complete gait cycle includes two foot-landing impacts. One is associated with the foot landing of the swing-foot heel when the domain switches from UA to OA, and the other is associated with the foot landing of the leading-foot toe when the domain switches from OA to FA. The domain switching from FA to UA is a smooth transition and thus does not involve any impact. At a foot-landing impact, the robot's joint positions will remain continuous, but its joint velocities will experience a sudden jump [6]. The impact dynamics can be described by the following reset map

$$\dot{\mathbf{q}}^+ = \mathbf{R}_{\dot{\mathbf{q}}}(\mathbf{q})\dot{\mathbf{q}}^-, \tag{5}$$

where $\dot{\mathbf{q}}^-$ and $\dot{\mathbf{q}}^+$ represent the values of $\dot{\mathbf{q}}$ right before and after an impact, respectively. Here, $\mathbf{R}_{\dot{q}} : Q \to \mathbb{R}^{(n+3)\times(n+3)}$ can be obtained by solving

$$\begin{bmatrix} \mathbf{M}(\mathbf{q}) & -\mathbf{J}^T(\mathbf{q}) \\ \mathbf{J}^T(\mathbf{q}) & \mathbf{0}_{p\times p} \end{bmatrix} \begin{bmatrix} \dot{\mathbf{q}}^+ \\ \delta\mathbf{F} \end{bmatrix} = \begin{bmatrix} \mathbf{M}(\mathbf{q})\dot{\mathbf{q}}^- \\ \mathbf{0}_{p\times 1} \end{bmatrix},$$

where $\delta\mathbf{F}$ is a vector of the impulsive external force, and $\mathbf{0}_{p\times p}$ is a $p\times p$ zero matrix. Here, p is the dimension of the external force. At the UA-to-OA impact, $p = 2$, which corresponds to the forward and vertical directions of the heel contact point of the swing foot. At the OA-to-FA impact, $p = 1$, which corresponds to the vertical direction of the swing-foot toe.

2 MODEL-BASED CONTROLLER DESIGN

In this study, the main control object is to achieve satisfactory tracking of the desired global-position trajectory for planar multi-domain bipedal robotic walking. To realize this objective, a model-based state feedback controller is developed based on the full-order dynamic model presented in the previous section.

To illustrate the proposed controller design, a planar bipedal robot with 6 revolute joints (i.e., $n = 6$) and 6 independent actuators (i.e., $n_a = 6$) is considered (see Fig. 2).

© 2019 by ASME

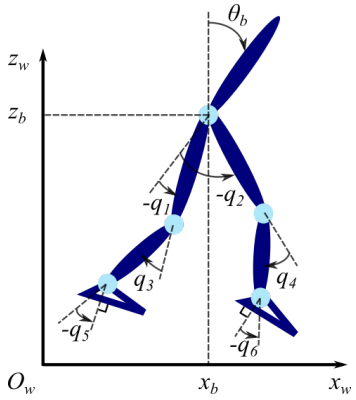

FIGURE 2. An illustration of the planar bipedal robot considered in the simulation. O_w, x_w, and z_w represent the origin, horizontal axis, and vertical axis of the world coordinate frame, respectively.

2.1 Trajectory Tracking Errors

Fully-Actuated Domain: Let $\mathbf{h}_{cF}(\mathbf{q}) : Q \to Q_c \subset \mathbb{R}^{n_a}$ denote the variables of interest to be controlled within the FA domain, which include: a) the robot's global position and orientation, represented by the floating-base coordinates, (x_b, z_b, θ_b); and b) the swing-foot position and orientation, denoted as $\mathbf{p}_{sw}(\mathbf{q}) \in \mathbb{R}^2$ and $\boldsymbol{\gamma}_{sw}(\mathbf{q}) \in \mathbb{R}$, respectively. Accordingly, $\mathbf{h}_{cF}(\mathbf{q})$ can be expressed as:

$$\mathbf{h}_{cF}(\mathbf{q}) := \left[x_b, z_b, \theta_b, \mathbf{p}_{sw}^T(\mathbf{q}), \gamma_{sw}^T(\mathbf{q})\right]^T. \tag{6}$$

Let $\mathbf{h}_{dF}(t, \theta(\mathbf{q})) : \mathbb{R}^+ \times \mathbb{R} \to \mathbb{R}^{n_a}$ denote the desired trajectories of $\mathbf{h}_{cF}(\mathbf{q})$ within the FA domain, which are encoded by time t and a configuration-based phase variable $\theta : Q \to Q_f \subset R$ that monotonically increases within a step and represents how far a step has progressed. Here, the desired global-position trajectory is defined as explicitly time-dependent because it is often expressed as time functions in practical robotic applications.

For the planar bipedal robot as shown in Fig. 2, the only feasible walking direction is along the x_w-axis of the world coordinate frame. Let $x_d(t)$ denote the desired global-position trajectory. Then, $\mathbf{h}_{dF}(t, \theta(\mathbf{q}))$ can be expressed as

$$\mathbf{h}_{dF}(t, \theta(\mathbf{q})) := [x_d(t), \boldsymbol{\phi}_F^T(\theta)]^T, \tag{7}$$

where $\boldsymbol{\phi}_F(\theta) : Q_f \to \mathbb{R}^{n_a-1}$ represents the desired trajectories of y_b, z_b, θ_b, $\mathbf{p}_{sw}$, and $\boldsymbol{\gamma}_{sw}$. Bézier polynomials can be used to parameterize the desired function $\boldsymbol{\phi}_F(\theta)$ as [7]

$$\boldsymbol{\phi}(s) := \sum_{k=0}^{M} \boldsymbol{\alpha}_k \frac{M!}{k!(M-k)!} s^k (1-s)^{M-k}, \tag{8}$$

where $s := \frac{\theta - \theta^+}{\theta^- - \theta^+}$ is the normalized phase variable, $\boldsymbol{\alpha}_k \in \mathbb{R}^{n_a-1}$ $(k = 0, 1, ..., M)$ is a coefficient vector that will be optimized in motion planning, θ^- and θ^+ denote the values of θ right before and after an impact associated with the desired gait, and M is the order of the Bézier polynomials.

From the above definitions, the trajectory tracking error can be expressed as

$$\mathbf{h}_F(t, \mathbf{q}) := \mathbf{h}_{cF}(\mathbf{q}) - \mathbf{h}_{dF}(t, \theta(\mathbf{q})).$$

Underactuated Domain: Let $\mathbf{h}_{cU}(\mathbf{q}) : Q \to Q_c \subset \mathbb{R}^{n_a}$ denote the variables of interest to be controlled within the UA domain, which are chosen as the individual joint angles of the robot. Thus, $\mathbf{h}_{cU}(\mathbf{q})$ is defined as:

$$\mathbf{h}_{cU}(\mathbf{q}) := \left[q_1, q_2, q_3, q_4, q_5, q_6\right]^T. \tag{9}$$

Let $\mathbf{h}_{dU}(\theta(\mathbf{q})) : Q_f \to \mathbb{R}^{n_a}$ denote the desired position trajectories of $\mathbf{h}_{cU}(\mathbf{q})$ within the UA domain. Note, within the UA domain, $\mathbf{h}_{dU}$ is independent of time because the robot's global position is not chosen as a controlled variable due to the lack of actuators to directly control all DOFs within the UA domain. However, the desired trajectories $\mathbf{h}_{dU}$ will be planned to agree with the desired global-position trajectory $x_d(t)$. Again, Bézier polynomials will be used to parameterize the desired function $\mathbf{h}_{dU}(\theta(\mathbf{q}))$.

From the above definitions, the trajectory tracking error can be expressed as

$$\mathbf{h}_U(\mathbf{q}) := \mathbf{h}_{cU}(\mathbf{q}) - \mathbf{h}_{dU}(\theta(\mathbf{q})).$$

Over-Actuated Domain: Let $\mathbf{h}_{cO}(\mathbf{q}) : Q \to Q_c \subset \mathbb{R}^{n_a-1}$ denote the variables of interest to be controlled within the OA domain, which include: a) the robot's global position and orientation, represented by the floating-base coordinates, (x_b, z_b, θ_b); and b) the orientation of the leading and trailing feet, which are denoted as $\theta_l(\mathbf{q}) \in \mathbb{R}$ and $\theta_t(\mathbf{q}) \in \mathbb{R}$, respectively. Thus, $\mathbf{h}_{cO}(\mathbf{q})$ is defined as:

$$\mathbf{h}_{cO}(\mathbf{q}) := \left[x_b, z_b, \theta_b, \theta_l(\mathbf{q}), \theta_t(\mathbf{q}),\right]^T. \tag{10}$$

Let $\mathbf{h}_{dO}(t, \theta(\mathbf{q})) : \mathbb{R}^+ \times Q_f \to \mathbb{R}^{n_a-1}$ denote the desired position trajectories of $\mathbf{h}_{cO}(\mathbf{q})$ within the OA domain. Similar to the FA domain, the desired trajectory $\mathbf{h}_{dO}(t, \theta(\mathbf{q}))$ can be expressed as

$$\mathbf{h}_{dO}(t, \theta(\mathbf{q})) := [x_d(t), \boldsymbol{\phi}_O^T(\theta(\mathbf{q}))]^T, \tag{11}$$

© 2019 by ASME

where $\boldsymbol{\phi}_O(\theta) : Q_f \to \mathbb{R}^{n_a-2}$ represents the desired trajectories of y_b, z_b, θ_b, θ_l and θ_t. Again, we can use Bézier polynomials to parameterize the desired function $\boldsymbol{\phi}_O(\theta)$.

From the above definitions, the trajectory tracking error can be expressed as

$$\mathbf{h}_O(t,\mathbf{q}) := \mathbf{h}_{cO}(\mathbf{q}) - \mathbf{h}_{dO}(t,\theta(\mathbf{q})).$$

2.2 Impact Invariance Condition

Since bipedal robotic walking inherently involves impacts between a landing foot and the ground, the desired trajectories $\mathbf{h}_{di}$ $(i \in \{F,U,O\})$ should respect the reset map in Eq. (5) [24]. To meet this requirement, a set of time-dependent impact invariance conditions will be derived.

Suppose that the three phases of the k^{th} step ($k \in \{1,2,...\}$) are sequenced in the order of

$$FA \to UA \to OA.$$

Let T_{3k-3}, T_{3k-2}, T_{3k-1}, and T_{3k} denote the actual initial moment, the $FA \to UA$ switching moment, the $UA \to OA$ switching moment, and the final moment of the k^{th} step, respectively. Let τ_{3k-3}, τ_{3k-2}, τ_{3k-1}, and τ_{3k} denote the corresponding desired switching moments. The time-dependent impact invariance conditions are satisfied if the following equations

$$\begin{aligned}
&\mathbf{h}_F(\tau_{3k-3},\mathbf{q}(\tau^+_{3k-3})) = \mathbf{0}; \quad \dot{\mathbf{h}}_F(\tau_{3k-3},\mathbf{q}(\tau^+_{3k-3}),\dot{\mathbf{q}}(\tau^+_{3k-3})) = \mathbf{0};\\
&\mathbf{h}_U(\tau_{3k-2},\mathbf{q}(\tau^+_{3k-2})) = \mathbf{0}; \quad \dot{\mathbf{h}}_U(\tau_{3k-2},\mathbf{q}(\tau^+_{3k-2}),\dot{\mathbf{q}}(\tau^+_{3k-2})) = \mathbf{0}; \quad (12)\\
&\mathbf{h}_O(\tau_{3k-1},\mathbf{q}(\tau^+_{3k-1})) = \mathbf{0}; \quad \dot{\mathbf{h}}_O(\tau_{3k-1},\mathbf{q}(\tau^+_{3k-1}),\dot{\mathbf{q}}(\tau^+_{3k-1})) = \mathbf{0},
\end{aligned}$$

automatically hold when the trajectory tracking errors and their derivatives are both zero right before the switching moments.

2.3 Model-based State Feedback Control

To simplify the complex dynamics of multi-domain bipedal robotic walking, input-output linearization is applied within each domain to linearize their nonlinear, time-varying continuous dynamics into a linear, time-invariant system. The output functions are defined as the trajectory tracking errors as derived in Section 2.1. Since the tracking error is a function of time t and configuration variable $\mathbf{q}$ within the FA and UA domains and is only a function of $\mathbf{q}$ within the underactuated domain, the expressions of the control laws are different for the three domains.

Fully-Actuated and Over-Actuated Domains: The output functions are defined as the trajectory tracking errors as derived in Section 2.1, i.e.,

$$\mathbf{y}_i = \mathbf{h}_i(t,\mathbf{q})$$

with $i \in \{F,O\}$. The following input-output linearizing control law [25]

$$\mathbf{u}_i = (\tfrac{\partial \mathbf{h}_i}{\partial \mathbf{q}}\mathbf{M}^{-1}\bar{\mathbf{B}})^{-1}[(\tfrac{\partial \mathbf{h}_i}{\partial \mathbf{q}})\mathbf{M}^{-1}\bar{\mathbf{c}} + \mathbf{v}_i - \tfrac{\partial^2 \mathbf{h}_i}{\partial t^2} - \tfrac{\partial}{\partial \mathbf{q}}(\tfrac{\partial \mathbf{h}_i}{\partial \mathbf{q}}\dot{\mathbf{q}})\dot{\mathbf{q}}] \quad (13)$$

will linearize the continuous dynamics into

$$\ddot{\mathbf{y}}_i = \mathbf{v}_i.$$

By applying the following proportional-derivative (PD) control

$$\mathbf{v}_i = -\mathbf{K}_{p,i}\mathbf{y}_i - \mathbf{K}_{d,i}\dot{\mathbf{y}}_i,$$

where $\mathbf{K}_{p,i}$ and $\mathbf{K}_{d,i}$ are positive-definite diagonal matrices, one has

$$\ddot{\mathbf{y}}_\mathbf{i} = -\mathbf{K}_{p,i}\mathbf{y}_i - \mathbf{K}_{d,i}\dot{\mathbf{y}}_i.$$

Underactuated Domain: The output functions are defined as the trajectory tracking errors, i.e.,

$$\mathbf{y}_U = \mathbf{h}_U(\mathbf{q}).$$

The following input-output linearizing control law

$$\mathbf{u}_U = (\tfrac{\partial \mathbf{h}_U}{\partial \mathbf{q}}\mathbf{M}^{-1}\bar{\mathbf{B}})^{-1}[(\tfrac{\partial \mathbf{h}_U}{\partial \mathbf{q}})\mathbf{M}^{-1}\bar{\mathbf{c}} + \mathbf{v}_U - \tfrac{\partial}{\partial \mathbf{q}}(\tfrac{\partial \mathbf{h}_U}{\partial \mathbf{q}}\dot{\mathbf{q}})\dot{\mathbf{q}}] \quad (14)$$

will linearize the continuous dynamics into $\ddot{\mathbf{y}}_U = \mathbf{v}_U$. Again, by applying PD control $\mathbf{v}_U = -\mathbf{K}_{pU}\mathbf{y}_U - \mathbf{K}_{dU}\dot{\mathbf{y}}_U$, where $\mathbf{K}_{pU}$ and $\mathbf{K}_{dU}$ are positive-definite diagnal matrices, one has $\ddot{\mathbf{y}}_U = -\mathbf{K}_{pU}\mathbf{y}_U - \mathbf{K}_{dU}\dot{\mathbf{y}}_U$.

Although the proposed control laws in Eqs. (13) and (14) can exponentially drive the output functions to zero within the three domains under properly chosen PD control gains, the discrete impact dynamics in Eq. (5) cannot be directly controlled. Also, due to the utilization of input-output linearization and the lack of actuators to directly control all the DOFs during the UA domain, internal dynamics [25] exist within the UA domain, which cannot be directly controlled as well. Thus, both the impact dynamics and the UA-domain internal dynamics of the closed-loop control system will remain time-varying and strongly nonlinear under the proposed control laws. It is then necessary to analyze the stability of the overall hybrid closed-loop control system for deriving sufficient conditions under which the proposed control laws can provably guarantee the closed-loop stability and tracking performance.

© 2019 by ASME

3 CLOSED-LOOP STABILITY ANALYSIS

To provably guarantee satisfactory tracking of the desired trajectories in the presence of the uncontrolled, nonlinear, and time-varying internal dynamics and reset maps, this section presents the stability analysis of the hybrid dynamical system in Eqs. (4) and (5) under the proposed control laws in Eqs. (13) and (14). Since the problem of closed-loop tracking performance analysis can be solved by analyzing the closed-loop stability of the tracking error dynamics, we will formally establish sufficient conditions based on the construction of multiple Lyapunov functions [22] under which the proposed control strategies can guarantee the stability of the closed-loop tracking error dynamics.

Respectively define the states within the FA, UA, and OA domains as:

$$\mathbf{x}_F := \left[\mathbf{y}_F^T \ \dot{\mathbf{y}}_F^T\right]^T, \quad \mathbf{x}_U := \left[\boldsymbol{\eta}^T \ \boldsymbol{\xi}^T\right]^T, \quad \text{and} \quad \mathbf{x}_O := \left[\mathbf{y}_O^T \ \dot{\mathbf{y}}_O^T\right]^T,$$

where

$$\boldsymbol{\xi} := \left[\mathbf{y}_U^T \ \dot{\mathbf{y}}_U^T\right]^T \text{ and } \boldsymbol{\eta} := \left[\psi_{st} - \psi_{std} \ \dot{\psi}_{st} - \dot{\psi}_{std}\right]^T$$

represent the state associated with the output functions and the internal state within the UA domain, respectively. Here, ψ_{st} is the passive pitch angle of the stance foot, which corresponds to the internal state within the UA domain.

The closed-loop dynamics can be expressed as:

$$\Sigma_F : \begin{cases} \dot{\mathbf{x}}_F = \mathbf{A}_F \mathbf{x}_F & \text{if } (t, \mathbf{x}_F^-) \notin S_{F\to U}(t, \mathbf{x}_F) \\ \mathbf{x}_F^+ = \Delta_{F\to U}(t, \mathbf{x}_F^-) & \text{if } (t, \mathbf{x}_F^-) \in S_{F\to U}(t, \mathbf{x}_F) \end{cases}$$

$$\Sigma_U : \begin{cases} \begin{cases} \dot{\boldsymbol{\xi}} &= \mathbf{A}_\xi \boldsymbol{\xi} \\ \dot{\boldsymbol{\eta}} &= \mathbf{f}_\eta(\boldsymbol{\eta}, \boldsymbol{\xi}) \end{cases} & \text{if } (t, \mathbf{x}_U^-) \notin S_{U\to O}(t, \mathbf{x}_U) \\ (\boldsymbol{\xi}^+, \boldsymbol{\eta}^+) = \Delta_{U\to O}(t, \boldsymbol{\xi}^-, \boldsymbol{\eta}^-) & \text{if } (t, \mathbf{x}_U^-) \in S_{U\to O}(t, \mathbf{x}_U) \end{cases}$$

$$\Sigma_O : \begin{cases} \dot{\mathbf{x}}_O = \mathbf{A}_O \mathbf{x}_O & \text{if } (t, \mathbf{x}_O^-) \notin S_{O\to F}(t, \mathbf{x}_O) \\ \mathbf{x}_O^+ = \Delta_{O\to F}(t, \mathbf{x}_O^-) & \text{if } (t, \mathbf{x}_O^-) \in S_{O\to F}(t, \mathbf{x}_O) \end{cases} \tag{15}$$

where

$$\mathbf{A}_F := \begin{bmatrix} \mathbf{0}_{n_a\times n_a} & \mathbf{I}_{n_a\times n_a} \\ -\mathbf{K}_{pF} & -\mathbf{K}_{dF} \end{bmatrix},$$

$$\mathbf{A}_\xi := \begin{bmatrix} \mathbf{0}_{n_a\times n_a} & \mathbf{I}_{n_a\times n_a} \\ -\mathbf{K}_{pU} & -\mathbf{K}_{dU} \end{bmatrix},$$

and

$$\mathbf{A}_O := \begin{bmatrix} \mathbf{0}_{(n_a-1)\times(n_a-1)} & \mathbf{I}_{(n_a-1)\times(n_a-1)} \\ -\mathbf{K}_{pO} & -\mathbf{K}_{dO} \end{bmatrix}.$$

Let $V_F(t, \mathbf{x}_F(t))$, $V_U(t, \mathbf{x}_U(t))$, and $V_O(t, \mathbf{x}_O(t))$ denote the Lyapunov function candidates during FA, UA, and OA domains, respectively. According to the stability conditions established in [22], the hybrid control system in Eq. (15) is stable in the sense of Lyapunov if the Lyapunov function candidates satisfy the following conditions:

(A1) Within the FA and OA domains, the Lyapunov function candidates V_F and V_O exponentially decrease, respectively.

(A2) Within the UA domain, the value of V_U right before "switching out" is bounded above by a continuous function of the value of V_U right after "switching-in".

(A3) The values of V_i at the "switching-in" moments form a non-increasing sequence for all $i \in \{FA, UA, OA\}$.

The stability of the closed-loop error dynamics in Eq. (15) will be analyzed next in order to translate the above stability conditions into mathematically rigorous sufficient conditions that the proposed continuous control laws should satisfy.

For notational simplicity, $\star(T_{3k-j}^-) := \star|_{3k-j}^-$ will be used in the following stability analysis ($k \in \{1, 2, ...\}$ and $j \in \{0, 1, 2, 3\}$). Due to space limitations, a sketch of the stability analysis will be presented.

First, sufficient conditions for satisfying (A1) are derived.

With the continuous control laws in Eqs. (13) and (14), it can be proved that if the PD gains are chosen such that $\mathbf{A}_i$ is Hurwitz then the Lyapunov function candidates V_i can be constructed in a way that during FA and OA there exist positive constants r_i, c_{1i}, c_{2i}, and c_{3i} such that [25]

$$c_{1i}\|\mathbf{x}_i\|^2 \le V_i(t, \mathbf{x}_i) \le c_{2i}\|\mathbf{x}_i\|^2 \quad \text{and} \quad \dot{V}_i \le -c_{3i} V_i \tag{16}$$

hold for any $\mathbf{x}_i \in B_{r_i}(\mathbf{0}) := \{\mathbf{x}_i : \|\mathbf{x}_i\| \le r_i\}$, where $i \in \{F, O\}$. From Eq. (16), one has

$$V_F|_{3k-2}^- \le e^{-c_{3F}(T_{3k-2} - T_{3k-3})} V_F|_{3k-3}^+ \tag{17}$$

and

$$V_O|_{3k}^- \le e^{-c_{3O}(T_{3k} - T_{3k-1})} V_O|_{3k-1}^+. \tag{18}$$

Hence, the condition (A1) can be locally satisfied by properly choosing PD gains to ensure that $\mathbf{A}_O$ and $\mathbf{A}_F$ are both Hurwitz.

Now, we will derive sufficient conditions to satisfy (A2).

Due to the utilization of input-output linearization and the lack of actuators to directly control all degrees of freedom within UA, internal dynamics exist within the UA whose dynamics cannot be directly controlled. The Lyapunov function candidate V_U can be constructed as

$$V_U = V_\xi(\boldsymbol{\xi}) + \beta\|\eta\|^2, \tag{19}$$

© 2019 by ASME

where β is a positive number. Since the state $\boldsymbol{\xi}$ is directly controlled within the UA, V_ξ can be constructed in a way similar to V_A and V_O. If the PD gains within the UA are selected such that $\mathbf{A}_\xi$ is Hurwitz, then there exist positive numbers c_ξ, $c_{1\xi}$, $c_{2\xi}$, and $c_{3\xi}$ such that

$$c_{1\xi}\|\boldsymbol{\xi}\|^2 \le V_\xi(t,\boldsymbol{\xi}) \le c_{2\xi}\|\boldsymbol{\xi}\|^2 \quad \text{and} \quad \dot{V}_\xi \le -c_{3\xi}V_\xi \tag{20}$$

hold for any $\boldsymbol{\xi} \in B_{r_\xi}(\mathbf{0})$. From Eq. (20), one has

$$V_\xi|^-_{3k-1} \le e^{-c_{3\xi}(T_{3k-1}-T_{3k-2})}V_\xi|^+_{3k-2}. \tag{21}$$

From Eq. (15), one has

$$\boldsymbol{\eta}|^-_{3k-1} = \int_{T_{3k-2}}^{T_{3k-1}} \mathbf{f}_\eta(s,\boldsymbol{\eta}(s),\boldsymbol{\xi}(s))ds + \boldsymbol{\eta}|^+_{3k-2}. \tag{22}$$

Thus,

$$\begin{aligned}\|\boldsymbol{\eta}|^-_{3k-1}\|^2 &\le \|\int_{T_{3k-2}}^{T_{3k-1}} \mathbf{f}_\eta(s,\boldsymbol{\eta}(s),\boldsymbol{\xi}(s))ds\|^2 + \|\boldsymbol{\eta}|^+_{3k-2}\|^2 \\ &\le \int_{T_{3k-2}}^{T_{3k-1}} \|\mathbf{f}_\eta(s,\boldsymbol{\eta}(s),\boldsymbol{\xi}(s))\|^2 ds + \|\boldsymbol{\eta}|^+_{3k-2}\|^2\end{aligned} \tag{23}$$

Assume that there exist positive numbers k_f and r_η such that $\|\mathbf{f}_\eta(t,\boldsymbol{\eta}(t),\boldsymbol{\zeta}(t))\|$ is bounded above by k_f for all $(\boldsymbol{\eta},\boldsymbol{\zeta}) \in B_{r_\eta}(\mathbf{0})$ [26], i.e.,

$$\|\mathbf{f}_\eta(t,\boldsymbol{\eta}(t),\boldsymbol{\xi}(t))\| \le k_f. \tag{24}$$

Then,

$$\|\boldsymbol{\eta}|^-_{3k-1}\|^2 \le k_f^2(T_{3k-1}-T_{3k-2}) + \|\boldsymbol{\eta}|^+_{3k-2}\|^2. \tag{25}$$

Here, the upper bound of the duration of the UA phase, $T_{3k-1} - T_{3k-2}$, can be estimated as

$$\begin{aligned}|T_{3k-1}-T_{3k-2}| &= |T_{3k-1}-\tau_{3k-1}+\tau_{3k-1}-T_{3k-2}| \\ &\le |T_{3k-1}-\tau_{3k-1}| + \Delta_{\tau_U},\end{aligned} \tag{26}$$

where $\Delta_{\tau_U} := \tau_{3k-1} - T_{3k-2}$ is the nominal duration of the k^{th}-step UA phase. Based on our previous work [21], there exists a small positive number ε_U such that

$$|T_{3k-1}-\tau_{3k-1}| \le \varepsilon_U \Delta_{\tau_U}. \tag{27}$$

From Eqs. (25)-(27), one has

$$\|\boldsymbol{\eta}|^-_{3k-1}\| \le k_f(1+\varepsilon_U)\Delta_{\tau_U} + \|\boldsymbol{\eta}|^+_{3k-2}\|. \tag{28}$$

Thus, from Eqs. (19), (21), and (28), one has

$$\begin{aligned}V_U|^-_{3k-1} =& V_\xi|^+_{3k-1} + \beta\|\boldsymbol{\eta}|^+_{3k-1}\|^2 \\ \le& e^{-c_{3\xi}(T_{3k-1}-T_{3k-2})}V_\xi|^+_{3k-2} + 2\beta\|\boldsymbol{\eta}|^+_{3k-2}\|^2 \\ &+ 2\beta k_f^2(1+\varepsilon_U)^2\Delta^2_{\tau_U} \\ &\le 2V_U|^+_{3k-2} + 2\beta k_f^2(1+\varepsilon_U)^2 =: w_u(V_U|^+_{3k-2}).\end{aligned} \tag{29}$$

Because $w_u(V_U|^+_{3k-2})$ is a continuous function of $V_U|^+_{3k-2}$, the condition (A2) is satisfied for any $\mathbf{x}_U \in B_{r_U}(\mathbf{0})$ with $r_U := \max(r_\xi, r_\eta)$.

Lastly, to satisfy the stability condition (A3), i.e.,

$$\{V_F|^+_0, V_F|^+_3, ...\},\ \{V_U|^+_1, V_U|^+_4, ...\}, \text{ and } \{V_O|^+_2, V_O|^+_5, ...\}$$

are all nonincreasing sequences, sufficient conditions will be derived based on our previous work [20]. For space consideration, only $\{V_F|^+_0, V_F|^+_3, ...\}$ will be discussed.

Upon a switching event at $t = T_{3k-2}$, one has

$$\begin{aligned}\|\mathbf{x}_U|^+_{3k-2}\| =& \|\boldsymbol{\Delta}_{F\to U}(T_{3k-2},\mathbf{x}_F|^-_{3k-2})\| \\ \le& \|\boldsymbol{\Delta}_{F\to U}(T_{3k-2},\mathbf{x}_F|^-_{3k-2}) - \boldsymbol{\Delta}_{F\to U}(\tau_{3k-2},\mathbf{x}_F|^-_{3k-2})\| \\ &+ \|\boldsymbol{\Delta}_{F\to U}(\tau_{3k-2},\mathbf{x}_F|^-_{3k-2}) - \boldsymbol{\Delta}_{F\to U}(\tau_{3k-2},\mathbf{0})\| \\ &+ \|\boldsymbol{\Delta}_{F\to U}(\tau_{3k-2},\mathbf{0})\|.\end{aligned} \tag{30}$$

Since $\boldsymbol{\Delta}_{F\to U}$ is a continuously differentiable function in t and $\mathbf{x}_F$, there exists a positive number l_F and Lipschitz constants L_{tF} and L_{xF} such that

$$\begin{aligned}&\|\boldsymbol{\Delta}_{F\to U}(T_{3k-2},\mathbf{x}_F|^-_{3k-2}) - \boldsymbol{\Delta}_{F\to U}(\tau_{3k-2},\mathbf{x}_F|^-_{3k-2})\| \\ \le& L_{tF}|T_{3k-2}-\tau_{3k-2}|\end{aligned} \tag{31}$$

and

$$\begin{aligned}&\|\boldsymbol{\Delta}_{F\to U}(\tau_{3k-2},\mathbf{x}_F|^-_{3k-2}) - \boldsymbol{\Delta}_{F\to U}(\tau_{3k-2},\mathbf{0})\| \\ \le& L_{xF}\|\mathbf{x}_F|^-_{3k-2}\|\end{aligned} \tag{32}$$

hold for any $\mathbf{x}_F|^-_{3k-2} \in B_{l_F}(\mathbf{0})$. Similar to Eq. (27), there exists a small positive number ε_F such that

$$|T_{3k-2}-\tau_{3k-2}| \le \varepsilon_F \Delta_{\tau_F}, \tag{33}$$

where $\Delta_{\tau_F} := \tau_{3k-2} - T_{3k-3}$ is the nominal duration of the k^{th}-step FA phase. Also, if the impact invariance conditions derived

© 2019 by ASME

in Section 2.2 can be satisfied through motion planning, then

$$\|\mathbf{\Delta}_{F\to U}(\tau_{3k-2},\mathbf{0})\| = 0. \tag{34}$$

From Eqs. (30)-(34), one has

$$\|\mathbf{x}_U|_{3k-2}^{+}\| \le L_{tF}\varepsilon_F\Delta_{\tau F} + L_{xF}\|\mathbf{x}_F|_{3k-2}^{-}\|. \tag{35}$$

Similar to the above derivation, one can obtain that there exists a small positive number ε_O, positive numbers l_U and l_O, and Lipschitz constants L_{tU}, L_{xU}, L_{tO}, and L_{xO} such that

$$\|\mathbf{x}_O|_{3k-1}^{+}\| \le L_{tU}\varepsilon_U\Delta_{\tau U} + L_{xU}\|\mathbf{x}_U|_{3k-1}^{-}\| \tag{36}$$

and

$$\|\mathbf{x}_F|_{3k}^{+}\| \le L_{tO}\varepsilon_O\Delta_{\tau O} + L_{xO}\|\mathbf{x}_O|_{3k}^{-}\| \tag{37}$$

hold for any $\mathbf{x}_U|_{3k-1}^{-} \in B_{lU}(\mathbf{0})$ and $\mathbf{x}_O|_{3k}^{-} \in B_{lO}(\mathbf{0})$, respectively, where $\Delta_{\tau O}$ is the nominal duration of the k^{th}-step OA phase. From Eqs. (16) and (33), one has

$$\|\mathbf{x}_F|_{3k-2}^{-}\| \le \sqrt{\frac{c_{2F}}{c_{1F}}}e^{-\frac{c_{3F}}{2c_{2F}}(1+\varepsilon_F)\Delta_{\tau_F}}\|\mathbf{x}_F|_{3k-3}^{+}\| \tag{38}$$

and

$$\|\mathbf{x}_O|_{3k}^{-}\| \le \sqrt{\frac{c_{2O}}{c_{1O}}}e^{-\frac{c_{3O}}{2c_{2O}}(1+\varepsilon_O)\Delta_{\tau_O}}\|\mathbf{x}_O|_{3k-1}^{+}\|. \tag{39}$$

Therefore, one can prove that

$$\begin{aligned}\|\mathbf{x}_F|_{3k}^{+}\| \le\ & L_{tO}\varepsilon_O\Delta_{\tau O}\\ & + L_{xO}\Big(\sqrt{\frac{c_{2O}}{c_{1O}}}e^{-\frac{c_{3O}}{2c_{2O}}(1+\varepsilon_O)\Delta_{\tau_O}}\\ & \cdot (L_{tU}\varepsilon_U\Delta_{\tau U}\\ & + L_{xU}(k_f(1+\varepsilon_U)\Delta_{\tau_U}\\ & + L_{tF}\varepsilon_F\Delta_{\tau F}\\ & + L_{xF}\sqrt{\frac{c_{2F}}{c_{1F}}}e^{-\frac{c_{3F}}{2c_{2F}}(1+\varepsilon_F)\Delta_{\tau_F}}\|\mathbf{x}_F|_{3k-3}^{+}\|)))\end{aligned}. \tag{40}$$

Define

$$\begin{aligned}\bar{N} :=& L_{tO}\varepsilon_O\Delta_{\tau O} + L_{xO}\Big(\sqrt{\frac{c_{2O}}{c_{1O}}}e^{-\frac{c_{3O}}{2c_{2O}}(1+\varepsilon_O)\Delta_{\tau_O}}\\ & (L_{tU}\varepsilon_U\Delta_{\tau U} + L_{xU}(k_f(1+\varepsilon_U)\Delta_{\tau_U} + L_{tF}\varepsilon_F\Delta_{\tau F})))\end{aligned} \tag{41}$$

and

$$\begin{aligned}\bar{L} :=& L_{xO}\Big(\sqrt{\frac{c_{2O}}{c_{1O}}}e^{-\frac{c_{3O}}{2c_{2O}}(1+\varepsilon_O)\Delta_{\tau_O}}\\ & (L_{tU}\varepsilon_U\Delta_{\tau U} + L_{xU}(k_f(1+\varepsilon_U)\Delta_{\tau_U}\\ & + L_{xF}\sqrt{\frac{c_{2F}}{c_{1F}}}e^{-\frac{c_{3F}}{2c_{2F}}(1+\varepsilon_F)\Delta_{\tau_F}}\|\mathbf{x}_F|_{3k-3}^{+}\|))),\end{aligned} \tag{42}$$

then Eq. (40) can be rearranged into

$$\|\mathbf{x}_F|_{3k}^{+}\| \le \bar{N} + \bar{L}\|\mathbf{x}_F|_{3k-3}^{+}\|. \tag{43}$$

From Eq. (16), one then has

$$V_F|_{3k}^{+} \le c_{2F}(2\bar{N}^2 + \frac{2\bar{L}^2}{c_{1F}}V_F|_{3k-3}^{+}). \tag{44}$$

Thus, if the PD gains in each domain are chosen to be sufficiently fast such that $\frac{2c_{2F}\bar{L}^2}{c_{1F}}$ is less than 1 and $2c_{2F}\bar{N}^2$ is sufficiently close to 0, then the condition (A3) can be satisfied.

4 SIMULATION

In this section, the simulation results are presented to demonstrate the effectiveness of the proposed control strategy. The planar bipedal robot as shown in Fig. 2 is simulated.

In MATLAB simulations, the continuous control laws in Eqs. (13) and (14) are implemented using the full-order model in Eq. (4). The PD gains K_p and K_d are set to be the same for three domains ($K_p = 225$ and $K_d = 15$). Such a choice of PD gains will guarantee that $\mathbf{A}_i$ is Hurwitz for all $i \in \{F,U,A\}$, thus satisfying the condition (A1).

Without loss of generality, the original desired global-position trajectory is chosen as $x_d(t) = 0.2t - 0.14$ m. Due to the utilization of input-output linearization during the UA domain, internal dynamics will exist, which cannot be directly controlled and may result in a relatively large tracking error at the beginning of the OA domain. To reduce the magnitude of the control effort required to mitigate this initial tracking error, the desired global-position trajectory within the OA domain is modified such that it matches the actual trajectory at the initial moment of an OA phase and smoothly connects to the original desired trajectory in the middle of the OA phase. Let $\bar{x}_d(t)$ denote this modified desired global-position trajectory.

Figure 3 shows the simulation results of the proposed multi-domain global-position control, which indicates that the controller is able to drive the robot to the modified desired global-position trajectory despite the presence of the nonlinear, time-varying internal dynamics and reset maps that can not be directly controlled. Although the robot tracks the modified desired

 © 2019 by ASME

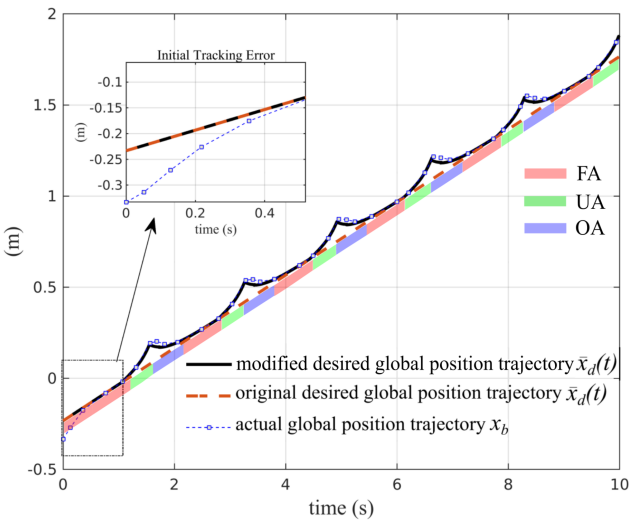

FIGURE 3. The global-position tracking performance of the proposed control strategy. Three walking domains are marked. The robot is able to converge to the modified desired global-position trajectory under a relatively large initial tracking error. Since the modified desired global-position trajectory is designed to stay sufficiently close to the original one, a bounded tracking error of the original desired trajectory is guaranteed.

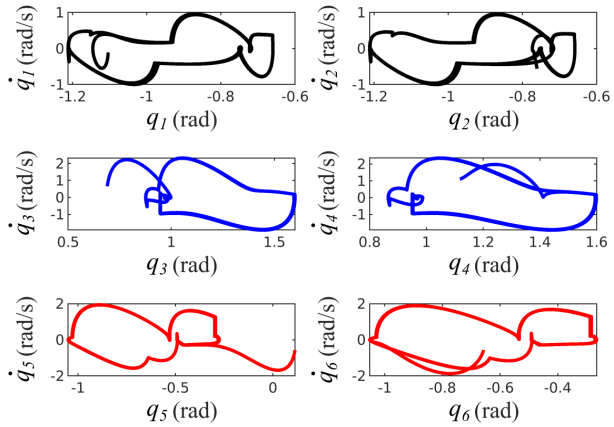

FIGURE 4. The phase portrait of robot's individual joint for 40 steps. It clearly shows that stable walking motions are realized under the proposed control approach.

global-position trajectory rather than the original one, we can still consider that satisfactory global-position tracking is realized because the modified desired trajectory is designed to overlap with the original one for the majority of the entire walking process.

Figure 4 shows the phase portrait of the robot's individual joint. It demonstrates that stable walking is realized in the presence of uncontrolled reset maps and internal dynamics.

5 CONCLUSIONS

This paper introduces a global-position tracking control approach for planar multi-domain bipedal robotic walking through full-order dynamic modeling, input-output linearizing state feedback control, and closed-loop stability analysis. The full-order dynamic model of a planar bipedal robot was represented, which describes the complete dynamic behaviors of all degrees of freedom for the robot during the three domains of multi-domain walking. The input-output linearization technique in combination with PD control was utilized to drive the output functions, which are defined as trajectory tracking errors, to zero within each domain. Despite the presence of uncontrolled internal dynamics and landing impact dynamics, the overall walking system can still reliably track the desired trajectories with bounded tracking errors. Simulations results demonstrated the effectiveness of the proposed walking strategy in realizing satisfactory global-position tracking for versatile multi-domain walking. In our future work, the proposed input-output linearizing control will be modified to guarantee robust trajectory tracking as well as to exploit the potential of multi-domain gait in achieving agile walking.

REFERENCES

[1] Lack, J., Powell, M. J., and Ames, A. D., 2014. "Planar multi-contact bipedal walking using hybrid zero dynamics". In Proc. International Conference on Robotics and Automation, pp. 2582–2588.

[2] Adamczyk, P. G., Collins, S. H., and Kuo, A. D., 2006. "The advantages of a rolling foot in human walking". *Journal of experimental biology,* **209**(20), pp. 3953–3963.

[3] Vukobratović, M., and Borovac, B., 2004. "Zero-Moment Point: thirty five years of its life". *International Journal of Humanoid Robotics,* **1**(01), pp. 157–173.

[4] Kajita, S., Nagasaki, T., Kaneko, K., and Hirukawa, H., 2007. "Zmp-based biped running control". *IEEE Robotics Automation Magazine,* **14**(2), June, pp. 63–72.

[5] Kim, J.-Y., Park, I.-W., and Oh, J.-H., 2006. "Experimental realization of dynamic walking of the biped humanoid robot khr-2 using zero moment point feedback and inertial measurement". *Advanced Robotics,* **20**(6), pp. 707–736.

[6] Grizzle, J. W., Abba, G., and Plestan, F., 2001. "Asymptotically stable walking for biped robots: Analysis via systems with impulse effects". *IEEE Transactions on Automatic Control,* **46**(1), pp. 51–64.

[7] Westervelt, E. R., Chevallereau, C., Choi, J. H., Morris, B., and Grizzle, J. W., 2007. *Feedback control of dynamic*

© 2019 by ASME

bipedal robot locomotion. CRC press.

[8] Ames, A. D., Cousineau, E. A., and Powell, M. J., 2012. "Dynamically stable bipedal robotic walking with NAO via human-inspired hybrid zero dynamics". In Proc. of ACM International Conference on Hybrid Systems: Computation and Control, pp. 135–144.

[9] Hereid, A., Cousineau, E. A., Hubicki, C. M., and Ames, A. D., 2016. "3D dynamic walking with underactuated humanoid robots: A direct collocation framework for optimizing hybrid zero dynamics". In Proc. of IEEE International Conference on Robotics and Automation, pp. 1447–1454.

[10] Chevallereau, C., Abba, G., Aoustin, Y., Plestan, F., Westervelt, E., De Wit, C. C., and Grizzle, J., 2003. "Rabbit: A testbed for advanced control theory". *IEEE Control Systems Magazine,* **23**(5), pp. 57–79.

[11] Zhao, H., Hereid, A., Ma, W.-l., and Ames, A. D., 2017. "Multi-contact bipedal robotic locomotion". *Robotica,* **35**(5), pp. 1072–1106.

[12] Hereid, A., Cousineau, E. A., Hubicki, C. M., and Ames, A. D., 2016. "3D dynamic walking with underactuated humanoid robots: A direct collocation framework for optimizing hybrid zero dynamics". In Proc. IEEE International Conference on Robotics and Automation, pp. 1447–1454.

[13] Zhao, H., Ma, W., Ames, A. D., and Zeagler, M. B., 2014. "Human-inspired multi-contact locomotion with amber2". In Proc. of ACM International Conference on Cyber-Physical Systems (ICCPS), pp. 199–210.

[14] Powell, M. J., Hereid, A., and Ames, A. D., 2013. "Speed regulation in 3D robotic walking through motion transitions between human-inspired partial hybrid zero dynamics". In Proc. of IEEE International Conference on Robotics and Automation, pp. 4803–4810.

[15] Da, X., Hartley, R., and Grizzle, J. W., 2017. "Supervised learning for stabilizing underactuated bipedal robot locomotion, with outdoor experiments on the wave field". In Proc. of IEEE International Conference on Robotics and Automation, pp. 3476–3483.

[16] Hereid, A., Harib, O., Hartley, R., Gong, Y., and Grizzle, J. W., 2018. "Rapid bipedal gait design using c-frost with illustration on a cassie-series robot". *arXiv preprint arXiv:1807.06614*.

[17] Agrawal, A., Harib, O., Hereid, A., Finet, S., Masselin, M., Praly, L., Ames, A. D., Sreenath, K., and Grizzle, J. W., 2017. "First steps towards translating hzd control of bipedal robots to decentralized control of exoskeletons". *IEEE Access,* **5**, pp. 9919–9934.

[18] Gu, Y., Yao, B., and Lee, C. G., 2016. "Bipedal gait recharacterization and walking encoding generalization for stable dynamic walking". In Proc. of IEEE International Conference on Robotics and Automation, pp. 1788–1793.

[19] Gu, Y., Yao, B., and Lee, C. G., 2018. "Exponential stabilization of fully actuated planar bipedal robotic walking with global position tracking capabilities". *Journal of Dynamic Systems, Measurement, and Control,* **140**(5), p. 051008.

[20] Gu, Y., Yao, B., and Lee, C. G., 2018. "Straight-line contouring control of fully actuated 3-D bipedal robotic walking". In Proc. of American Control Conference, pp. 2108–2113.

[21] Gao, Y., and Gu, Y. "Time-dependent global-position tracking control of a nao bipedal walking robot". In Proc. of American Control Conference.

[22] Branicky, M. S., 1998. "Multiple lyapunov functions and other analysis tools for switched and hybrid systems". *IEEE Transactions on Automatic Control,* **43**(4), pp. 475–482.

[23] The MathWorks, Inc. https://www.mathworks.com/. Accessed: 2019-03-20.

[24] Westervelt, E. R., Grizzle, J. W., and Koditschek, D. E., 2003. "Hybrid zero dynamics of planar biped walkers". *IEEE Transactions on Automatic Control,* **48**(1), pp. 42–56.

[25] Khalil, H. K., 1996. *Nonlinear systems*. Prentice Hall.

[26] Biemond, J. B., van de Wouw, N., Heemels, W. P. M., and Nijmeijer, H., 2013. "Tracking control for hybrid systems with state-triggered jumps". *IEEE Transactions on Automatic Control,* **58**(4), pp. 876–890.

© 2019 by ASME